Supplementary Information for

Quantum-Driven Anomalous Isotopic Effect at the Liquid Water-Oxide Interface

Huiling Chen[1*], Weizhong Fu[2*], Fanjin Lu[1*], Xin Lin[1], Xinyi Liu[1], Xiaoqun Li[3], Yuxuan Liu[1], Ji Chen[2,4✉], Wei-Tao Liu[1✉]
Corresponding author. Email: ji.chen@pku.edu.cn, wtliu@fudan.edu.cn

Table of content

S1. Basic principle of SFVS

The basic principle of sum-frequency generation (SFG) has been described elsewhere [55]. Briefly, when the infrared (IR) frequency (ω_{IR}) is near vibrational resonances, the sum-frequency (SF) signal (S_{SF}) generated by the incident beams follows:

$$S_{SF} \propto \left|\chi_{eff}^{(2)}\right| = |\chi_{NR} + \chi_R|^2 = \left|\chi_{NR} + \sum_q \frac{A_q}{\omega_{IR} - \omega_q + i\Gamma_q}\right|^2, \quad \text{(S1)}$$

where χ_{NR} and χ_R are the non-resonant and resonant contributions, respectively. The parameters A_q, ω_q, and Γ_q denote the amplitude, frequency, and damping coefficient of the q^{th} resonance mode, respectively. When considering inhomogeneous broadening, the SF output of Equation (S1) becomes [56]:

$$S_{SF} \propto \left|\chi_{NR} + \sum_q \int_{-\infty}^{\infty} \frac{A_q}{\omega_{IR} - \omega' + i\Gamma_q} \frac{1}{\sqrt{2\pi}\sigma_q} \exp\left(-\frac{(\omega' - \omega_q)^2}{2\sigma_q^2}\right) d\omega'\right|^2, \quad \text{(S2)}$$

where σ_q is the inhomogeneous bandwidth [56]. Figures S1a and S1b show the fits of the experimental SF spectra taken from the SiO_2/H_2O and SiO_2/D_2O interfaces at different pH (pD) values using Equation (S2). The fitting values of damping coefficients (Γ_q) and inhomogeneous bandwidths (σ_q) were ~43 and 27 cm^{-1} for the Si–OH (Si–OD) band, and ~45 and 28 cm^{-1} for the $Si–O^-$ band. The resonant amplitudes of the Si–OH (Si–OD) band, deduced from these fits, are plotted as a function of pH (pD) values in Fig. 1e of the main text. Additionally, the frequency shift of the Si–OH (Si–OD) band, relative to its frequency at pH (pD) = 2, is plotted against pH (pD) values in Fig. 1f of the main text.

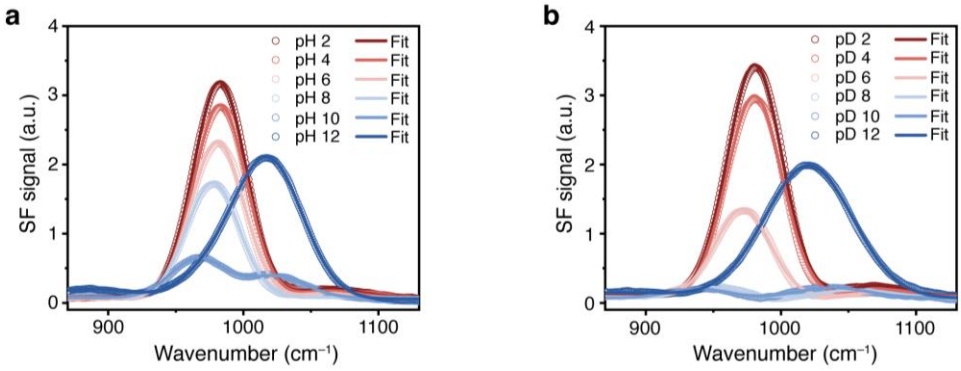

Figure S1 | Representative fits of SF spectra at varying pH (pD) values. a, SiO_2/H_2O interface; **b**, SiO_2/D_2O interface.

S2. Orientation of the interfacial Si–O bonds

For the SSP (S-SF, S-NIR, P-IR) and PPP (P-SF, P-NIR, P-IR) beam polarization combinations, the effective SF amplitudes for an anisotropic interface are given by [57]:

$$\begin{aligned} A_{SSP} &= \sin\beta_{IR}\, L_{yy}(\omega_{SF}) L_{yy}(\omega_{NIR}) L_{zz}(\omega_{IR}) A_{yyz}, \\ A_{PPP} &\approx -\cos\beta_{SF}\cos\beta_{NIR}\sin\beta_{IR}\, L_{xx}(\omega_{SF}) L_{xx}(\omega_{NIR}) L_{zz}(\omega_{IR}) A_{xxz} \\ &\quad + \sin\beta_{SF}\sin\beta_{NIR}\sin\beta_{IR}\, L_{zz}(\omega_{SF}) L_{zz}(\omega_{NIR}) L_{zz}(\omega_{IR}) A_{zzz}, \end{aligned} \tag{S3}$$

with β_n and $L_{ii}(\omega_n)$ being the beam incident angle and Fresnel coefficients, respectively. The coordinates $\{x, y, z\}$ refer to the laboratory frame, with the z-axis along the surface normal and the x-axis lying in the plane of incidence. For linear bonds on an azimuthally isotropic surface, the ratio between A_{PPP} and A_{SSP} is known to be sensitive to the bond's polar orientation [29].

The basic principle for extracting the orientation of an interfacial moiety from SFS has been described elsewhere [29,57]. Briefly, in the molecular coordinate system $\{a, b, c\}$, the c-axis is aligned parallel to the Si–O bond (Fig. S2a). The tilt angle θ of the Si–O bond relative to the surface normal is defined as the angle between the molecular c-axis and the laboratory z-axis. Assuming that the interfacial Si–O bonds are isotropically distributed in the surface plane, their net in-plane orientation averages to zero, and only the net out-of-plane orientation θ is considered. The non-vanishing elements of the hyperpolarizability tensor for the Si–O stretching vibrational mode are given by $\alpha_{aac} = \alpha_{bbc} = r\alpha_{ccc}$, with the Raman depolarization ratio r falling within the range of 0.1~0.3 for silica [58]. For an isotropic interface, the relationship between the SF amplitude A in the laboratory coordinates and the molecular hyperpolarizability α can be expressed as [59]:

$$\begin{aligned} A_{xxz} &= A_{yyz} = \frac{1}{2} N_s \alpha_{ccc} [(1+r)\cos\theta - (1-r)\cos^3\theta], \\ A_{zzz} &= N_s \alpha_{ccc} [r\cos\theta + (1-r)\cos^3\theta], \end{aligned} \tag{S4}$$

where N_s denotes the surface number density of contributing species, and θ represents the average tilt angle of the surface Si–O bonds.

By fitting the spectra with SSP (Figs. 1c and 1d) and PPP (Extended Data Fig. 2) beam polarization combinations and applying Eqs. (S3-S4), the orientations of the Si–OH and Si–OD bonds (assuming a δ-distribution) were deduced from the ratio A_{PPP}/A_{SSP} as a function of pH (pD) values, as shown in Fig. S2b. The results indicate that the Si–OH bond maintains an orientation within 25~34° from the surface normal across the pH range of 2~9, and the Si–OD bond remains oriented 23~28° from the surface normal across the pD range of 2~7 (Fig. S2b), both being very similar. This further rules out the influence of Si–O bond orientational changes on the observed isotope effect.

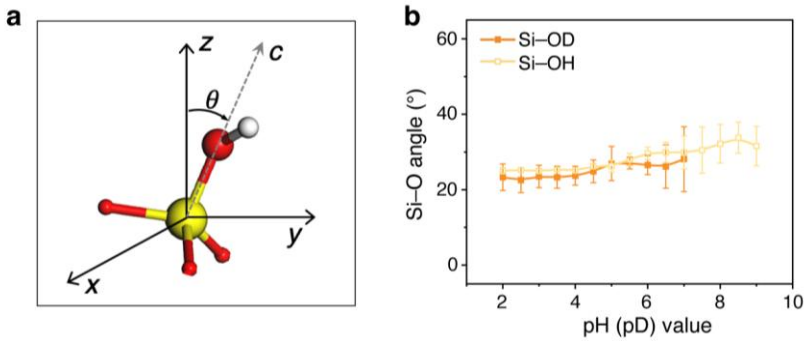

Figure S2 | Orientation distribution of Si–OH (Si–OD) bond. a, Illustration of an Si–O bond in the lab coordinates, θ is the tilting angle from the surface normal. **b**, Tilting angles of interfacial Si–OH and Si–OD bonds deduced from the A_{PPP}/A_{SSP} ratio obtained by fitting the SF spectra with PPP and SSP polarization combinations.

S3. *Ab initio* path integral MD simulations

The giant isotope effects observed in our experiments prompted us to perform *ab initio* path integral molecular dynamics (AI-PIMD) simulations on the SiO_2/water interface (Fig. S3a) to uncover the underlying nuclear quantum effects (NQEs). Our simulations reveal that NQEs induce different degrees of proton delocalization under different circumstances at the SiO_2/water interface (Fig. S3b), providing a plausible explanation for the observed giant isotope effects.

We first calculated a neutral aqueous interface with H_2O (*i.e.* without taking the proton out of the system) as a benchmark. This simulation was conducted for 40 ps, while other simulations were performed approximately 25 ps. During deprotonation in the neutral H_2O system, the protons transfer actively (Fig. S3c). Prior to deprotonation, one standing Si–OH group rotates down into the plane (Fig. S3d, red line), resulting in an excess in-plane proton. This new in-plane proton pulls two oxygen atoms closer together, decreasing their separation from 3.3 Å to 2.5 Å. At aroud 29 ps, a deprotonation event occurrs (Fig. S3d, green line).

The simulated trajectory can be divided in two parts: before and after Si–OH deprotonation. Before Si–OH dissociation occurs, the interfacial H/O ratio in the model is 8:8. The distribution of δ shows typical behavior for the Si–OH group, with δ peaking at ~0.40 Å (Fig. S3b, blue solid line). In the two-dimensional contour plot of δ and oxygen-oxygen distance (r_{OO}) (Fig. 2d, main text), we observed that the distribution of δ is correlated with r_{OO}, peaking at ~2.50 Å. After deprotonation, the interfacial H/O ratio changes to 7:8, and the water regime in our simulation becomes acidic. In this case, one proton can be fully shared by a pair of Si–O pair, featuring a probability distribution of δ peaking at 0 (Fig. S3b, green solid line). We also observe that proton-sharing is accompanied by a decrease in r_{OO} to 2.44 Å (Fig. 2g, main text). For comparison, a same model with D_2O was simulated, but no de-deuteration occurs. Due to the reduced NQEs, both δ and r_{OO} increase (Fig. S3b, blue dotted line; Fig. 2c, main text).

Inspired by the experimental observation that deprotonation is sensitive to the acidity of the solution, we conducted another set of simulation in which one proton was removed from the system. This automatically results in a Si–OH and Si–O^- pair, wtih an interfacial H/O ratio of 7:8, while there is no excessive charge in the water regime . In this system, the proton shows a partial sharing feature (Fig. S3b, orange solid line). Instead of complete proton-sharing, the proton still favors bonding more closely with one Si–O group than the other. However, compared to the undeprotonated system, the number of instantaneous configurations where the proton is shared (δ = 0) increase significantly, with r_{OO} approaching 2.45 Å (Fig. S3b, orange solid line; Fig. 2f, main text). The most probable configurtion occurs at δ = 0.39 Å and r_{OO} = 2.50 Å (Fig. S3b, orange solid line; Fig. 2f, main text). Furthermore, simulations with D_2O on this system show that, with deuterium substitution, NQEs become weaker. Consequently, we observe a weaker proton-sharing feature in D_2O than in H_2O (Fig. S3b, orange dotted line; Fig. 2e, main text).

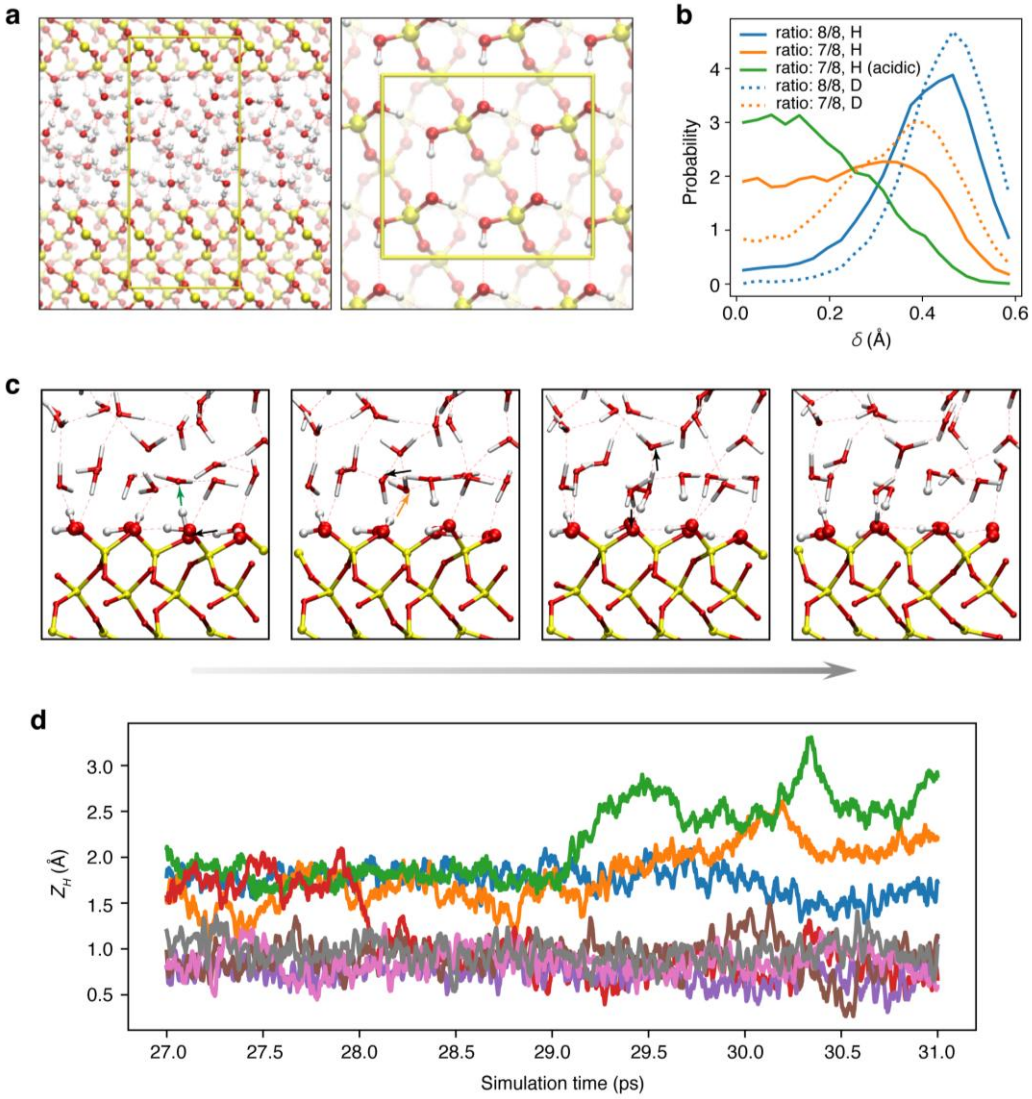

Figure S3 | Simulation detials and proton delocalization at the SiO_2/water interface. a, Side view (left) from a representative snapshot of the AI-PIMD simulations and top view (right) of a dry hydroxylated α-quartz surface. Hydrogen, oxygen, and silicon atoms are colored in white, red, and yellow, respectively. The surface unit cell is outline in yellow. **b**, Degree of proton delocalization under different circumstances. The parameter "ratio" refers to the number ratio of interfacial protons to oxygen atoms, and "acidic" denotes the presence of a hydronium ion in bulk water. **c**, Time-sequenced snapshots along the AI-PIMD trajectory at the SiO_2/H_2O interface, depicting a representative proton dissociation and migration event (trajectory indicated by grey arrow). The surface silanol group and proton involved in the process are highlighted in ball-and-stick representation, while the surrounding molecules are shown as sticks. Arrows trace the proton transfer pathway, where the proton-sharing center diffuses across several unit cells with the assistance of interfacial water molecules. **d**, Time evolution of the height of interfacial protons relative to the height of oxygen atoms on the surface.

References

55. Shen, Y. R., *Fundamentals of Sum-Frequency Spectroscopy*. (Cambridge University Press, Cambridge, 2016).
56. Ostroverkhov, V., Waychunas, G. A. & Shen, Y. R. Vibrational spectra of water at water/alpha-quartz (0001) interface. *Chem. Phys. Lett.* **386**, 144-148 (2004).
57. Yang, D. *et al.*. Facet-specific interaction between methanol and TiO_2 probed by sum-frequency vibrational spectroscopy. *Proc. Natl. Acad. Sci. U. S. A.* **115**, E3888-E3894 (2018).
58. McMillan, P. F. Structural studies of silicate glasses and melt?applications and limitations of Raman spectroscopy. *Am. Mineral.* **69**, 622-644 (1984).
59. Wang, H., Velarde, L., Gan, W. & Fu, L. Quantitative sum-frequency generation vibrational spectroscopy of molecular surfaces and interfaces: Lineshape, polarization, and orientation. *Annu. Rev. Phys. Chem.* **66**, 189-216 (2015).